On quantum effects near the liquid–vapor transition in helium

Martin H. Müser
Institut für Physik, WA 331, Johannes Gutenberg-Universität, D-55099 Mainz, Germany

Erik Luijten[a)]
Institute for Physical Science and Technology, University of Maryland, College Park, Maryland 20742-2431

The liquid–vapor transition in ^{3}He and ^{4}He is investigated by means of path-integral molecular dynamics and the quantum virial expansion. Both methods are applied to the critical isobar and the critical isochore. While previous path-integral simulations have mainly considered the lambda transition and superfluid regime in ^{4}He, we focus on the vicinity of the critical point and obtain good agreement with experimental results for the molar volume and the internal energy down to subcritical temperatures. We find that an effective classical potential that properly describes the two-particle radial distribution function exhibits a strong temperature dependence near the critical temperature. This contrasts with the behavior of essentially classical systems like xenon, where the effective potential is independent of temperature. It is conjectured that, owing to this difference in behavior between classical and quantum-mechanical systems, the crossover behavior observed for helium in the vicinity of the critical point differs qualitatively from that of other simple liquids. © *2002 American Institute of Physics.* [DOI: 10.1063/1.1429957]

I. INTRODUCTION

Crossover phenomena have enjoyed a renewed attention in recent years, both from the theoretical (see, e.g., Refs. 1–5) and from the experimental side (cf. Refs. 6–8); see also Ref. 9 and references therein. This concerns in particular the crossover from mean-field-like to Ising-type critical behavior upon approach of the critical point. The accurate numerical determination of crossover scaling functions for the isothermal compressibility and the liquid–vapor coexistence curve[10] has motivated the reexamination of experimental data for ^{3}He and Xe.[11] Xenon, with a very high molar mass and a relatively high critical temperature, is essentially a classical system, while the critical point for ^{3}He occurs at a temperature and density where quantum effects are expected to be non-negligible. This is also expressed by the de Boer parameter Λ^*.[12] For monatomic gases of atomic mass m, that are described by a Lennard-Jones potential with parameters ε and σ, this parameter is defined as $\Lambda^* = h/\sigma\sqrt{m\varepsilon}$. For ^{3}He its value is $\Lambda^* = 3.08$, compared to $\Lambda^* = 0.064$ for xenon.[13] Nevertheless, the nature of the critical point itself is the same for both fluids, because the critical fluctuations dominate over the quantum-mechanical fluctuations at temperatures sufficiently close to the critical temperature T_c. Thus, the values of the critical exponents are not affected. For the crossover region, the situation is less clear-cut. Since the correlation length now has a finite (although large) value, nonuniversal behavior may be expected for different systems and has actually been observed.[7] However, according to theory, this nonuniversality is largely determined by the so-called cutoff parameter (the wave number corresponding to some microscopic characteristic length) which in most

simple fluids has a very similar value.[7] Furthermore, also in numerical simulations of Ising-type systems a high degree of universality has been observed for crossover scaling functions.[14] Thus, it came as quite a surprise that the crossover behavior for ^{3}He exhibits a marked difference from that of xenon.[11] Owing to the short range of the interactions, these systems cannot be expected to complete the full crossover to mean-field-like behavior before leaving the critical region [where $t \ll 1$, with $t \equiv (T - T_c)/T_c$]. Nevertheless, for $T > T_c$ the crossover behavior of the isothermal compressibility of xenon turned out to agree very well with the numerical data for the three-dimensional Ising model with varying interaction range,[10] whereas the corresponding experimental data for ^{3}He seemed to be described by a *qualitatively different* curve. For $t \gtrsim 0.01$, the compressibility appeared essentially *suppressed* compared to the crossover scaling function. In Ref. 11, this difference in behavior was conjectured to be related to quantum-mechanical effects: The critical compressibility of ^{3}He would be enhanced due to quantum fluctuations, which are temperature dependent. Hence, this contribution is expected to decrease appreciably within the (high-temperature) crossover region, effectively leading to an additional reduction of the compressibility upon increase of the temperature. Clearly, it is only the compressibility due to the thermal fluctuations which is described by the various theoretical expressions for the crossover scaling function.

In order to gauge the quantum-mechanical contribution to the compressibility, a comprehensive theoretical description of the critical behavior, *including* the role of quantum effects, is required; such a description should encompass the temperature dependence of this contribution in the vicinity of T_c. Indeed, for a weakly interacting Bose fluid a scaling function has been calculated describing the crossover from

[a)]Presently at Department of Materials Science and Engineering, University of Illinois, Urbana, IL 61801. Electronic mail: luijten@uiuc.edu

criticality (i.e., the lambda point) to ideal Bose-gas behavior.[15,16] In particular, it was found that a mapping of the Hamiltonian for the Bose gas onto a classical spin model yields a Landau–Ginzburg–Wilson Hamiltonian with a quartic term that has a strongly temperature-dependent coefficient.[15] Since this coefficient plays a pivotal role in crossover scaling functions, a corresponding effect in the vicinity of the liquid–vapor critical point would definitely affect the nature of the crossover from Ising-type to mean-field-like critical behavior. These considerations have motivated us to examine the behavior of helium close to the critical point by means of quantum-mechanical numerical methods. In particular, it is of interest to see whether the magnitude of quantum effects indeed changes appreciably over the crossover region, as conjectured in Ref. 11. In the present study, we pay some attention to ^{3}He, but our main focus is on ^{4}He. Due to the higher mass of ^{4}He, quantum effects are less pronounced, which is only reinforced by the correspondingly higher critical temperature. This facilitates the numerical calculations considerably, as will be outlined in Sec. II A. At the same time, the quantum effects are still clearly visible in the crossover region and the isothermal compressibility indeed exhibits a deviation from the predicted crossover curve, similar to that found for ^{3}He.[11] For comparison, ^{4}He has a de Boer parameter $\Lambda^* = 2.67$, compared to the above-mentioned value $\Lambda^* = 3.08$ for ^{3}He.[13]

For completeness we remark that ^{4}He has been extensively studied by means of the path-integral Monte Carlo method, especially in the context of the lambda transition taking place at 2.17 K; cf. Ref. 17. Also, the high-density region has been explored in this way,[18] but we are not aware of numerical studies in the vicinity of the liquid–vapor critical point.

The outline of this paper is as follows. In Sec. II we introduce the methods that we have applied: Path-integral molecular dynamics is discussed in Sec. II A, followed by the quantum virial expansion in Sec. II B. Section III contains all our main results, namely data for the atomic volume of ^{4}He and for its kinetic, potential, and internal energy along the critical isobar, as well as for the kinetic and potential energy of ^{4}He and ^{3}He along their respective critical isochores. Furthermore, results for the effective pair potential of ^{3}He in the vicinity of the critical temperature are presented. Our conclusions are summarized in Sec. IV.

II. METHODS

A. Path-integral molecular dynamics

Path-integral Monte Carlo (PIMC)[19,20] and path-integral molecular dynamics (PIMD)[21] are well-established methods to calculate thermodynamic properties of many-particle quantum systems. Path-integral techniques exploit the possibility to represent the quantum-mechanical partition function of point particles as a classical partition function of closed polymers.[17] Neighboring beads in the polymer are coupled via elastic springs with stiffness $k = mM^2/\beta^2\hbar^2$, where m is the mass of the point particle, the so-called Trotter number M represents the number of beads in the polymer, and $\beta = 1/k_B T$. Interaction between polymers only takes place be-

tween those monomers that have the same index within the respective polymers to which they belong, and the effective temperature in the isomorphic classical representation is given by TM. For more details, we refer the reader to the original literature and review articles.[17,19,22,23]

Depending on the nature of the problem under study, Monte Carlo methods are preferable to molecular dynamics or vice versa. PIMC has so far been the method of choice for finite-temperature simulations of condensed helium, in particular when exchange effects played an important role. Far away from the superfluid regime, however, exchange effects can be neglected,[17] so that PIMC is not necessarily advantageous to PIMD for the study of the liquid–vapor transition. For example, in the gas phase, ballistic trajectories can be realized in PIMD, which allows rapid changes in the configuration. In conventional Monte Carlo methods, motions are constrained to be diffusive and large correlation times may be expected. Also, in isobaric simulations volume moves are done at no extra cost in a molecular dynamics simulation, while Monte Carlo methods require the evaluation of the total energy of the system.

Using an appropriate representation of the internal coordinates of the chain molecules, it is possible to avoid inefficient sampling;[21] e.g., in the regular representation, where each bead in a chain has the same dynamical inertia, the time-step discretization has to be chosen proportional to M^{-2}. In this study, we have used a representation of the chain molecules in terms of the center-of-mass coordinate and the eigencoordinates of the free particles, defined in Eq. (3) below, which makes it possible to work with time steps independent of M. While the "dynamical" center-of-mass coordinate is chosen to be identical with the real mass m, different masses m_q are attributed to each eigenmode q. An efficient choice is $m_q = (\tilde{k} + k_q)m/\tilde{k}$, where $\tilde{k}$ is an adjustable parameter and k_q is the stiffness associated with the eigenmode q. $\tilde{k}$ is conveniently chosen such that in the condensed phase all modes move on approximately the same time scale.

A disadvantage of PIMD is that for a fixed *dynamic* time step Δt, errors due to the finiteness of Δt may increase linearly with increasing Trotter number M. In such a case the round-off errors increase with decreasing *imaginary* time step β/M. While the radial distribution function, the average potential energy, and the virial estimator for the kinetic energy[24] do not suffer noticeably from this effect in our PIMD simulations, the so-called primitive estimator for the kinetic energy, K_{prim}, does. Thus, the typical systematic error in K_{prim} due to finite Δt is M times larger than that in the virial estimator. An estimator is a function whose *average* value corresponds to the expectation value of a property of interest. For an *individual* configuration, however, the association of the actual value of the estimator with the actual value of the property is meaningless. K_{prim} is given by[24]

$$K_{\text{prim}} = \frac{3}{2}Nk_B T M^2 - \frac{k}{2}\sum_{i=1}^{N}\sum_{\tau=1}^{M}(\mathbf{r}_{i\tau} - \mathbf{r}_{i\tau+1})^2, \qquad (1)$$

where $\mathbf{r}_{i\tau}$ represents the position of the τth monomer in polymer i, and k is the stiffness introduced at the beginning of this section. In addition to the above-mentioned systematic

error, K_{prim} has been shown to have large statistical errors for large Trotter numbers M, even in PIMC simulations.[24] However, a simple trick remedies both of these shortcomings.[25] If $\frac{3}{2}Nk_BTM^2$ is replaced by the actual "dynamic" kinetic energy, a new estimator can be defined

$$\tilde{K}_{\text{prim}} = \frac{1}{2} \sum_{i=1}^{N} \sum_{q=1}^{M} (m_q \mathbf{v}_{iq}'^2 - k_q \mathbf{r}_{iq}'^2), \qquad (2)$$

where $\mathbf{v}_{iq}'$ denotes the velocity associated with the eigencoordinate

$$\mathbf{r}_{iq}' = \frac{1}{\sqrt{M}} \sum_{\tau=1}^{M} \mathbf{r}_{i\tau} e^{2\pi i q\tau/M}. \qquad (3)$$

For methods to perform PIMD simulations at constant pressure, we refer to Refs. 25 and 26.

All simulations, as well as the virial expansions, are based on the Aziz HFD-B potential,[27] which is considered one of the best-known interatomic model potentials.[17] It consists of a Hartree–Fock (exponential) short-range repulsive term and algebraic long-range attractive terms ($1/r^6$, $1/r^8$, $1/r^{10}$). Recently, efforts have been devoted to incorporating three-body effects into the helium potential energy surface.[28] However, even for atomic volumes as small as 25 Å^3, there seems to be little deviation between the Aziz HFD-B potential and the three-body potential of Moroni et $al.$ (see, e.g., the 2% difference for the kinetic energy of solid ^{3}He shown in Fig. 6 of Ref. 25). We may thus safely assume that the Aziz HFD-B potential is adequate for the description of less dense systems, like those studied here. Furthermore, we note that it has been used very successfully in simulations of fluid and superfluid helium, as discussed in the well-known review of Ceperley.[17] The cutoff radius that we used in our simulations was $r_c = 10$ Å. The particle number in all simulations was $N = 500$ and the Trotter number varied between $M = 1$ for classical simulations and $M = 64$ for the quantum-mechanical ^{4}He simulations at the lowest temperatures, keeping $TM > 200$ K. The usual corrections of the order of $1/M^2$ were applied to the final data.[29] For the ^{3}He simulations, $TM > 350$ K was used with a maximum value of $M = 128$. We have used a cubic simulation box with periodic boundary conditions; the length of each simulation amounted to at least 50 000 time steps.

Note that our simulations mostly address the identification of quantum effects in the first derivatives of the thermodynamic potential (internal energy, volume, etc.), while an estimation of second derivatives such as the compressibility (discussed in Ref. 11) is not attempted: This would require much larger system sizes and is not feasible with our computer resources.

Exchange effects were neglected in our study. This leads to significant errors in the energy of the liquid in the superfluid phase and its vicinity. The order of magnitude of these errors may be estimated by integrating the λ peak in the specific heat, which yields an energy of about 1 K. However, near the critical temperature, exchange effects will be smaller and we follow an alternative route to estimate these by calculating the virial coefficient B_2 (see Sec. II B for more details). It turns out that in the temperature regime investigated, B_2 is larger for the bosonic case than if two ^{4}He atoms are treated as distinguishable. The bosonic case can be treated by restricting the evaluation of Eq. (9) to even angular momenta. The effect in B_2 (and $\partial B_2/\partial \beta$) is approximately 14% at $T = 3$ K and approximately 10% at $T = 7$ K. Therefore, in this temperature regime the difference between bosonic ^{4}He and "distinguishable" ^{4}He in the leading corrections to the ideal-gas behavior is of the order of 10%.

Its lower mass and lower liquid–gas transition temperature will make exchange effects more important for ^{3}He than for ^{4}He. On the other hand, there is significant cancellation of exchange effects in ^{3}He: If two spin-up ^{3}He atoms form a dimer, the spin wave function will be symmetric while the real-space wave function will be antisymmetric (fermionic). However, if a spin-up ^{3}He and a spin-down ^{3}He form a dimer, the opposite will happen: The spin wave function will be antisymmetric and the real-space wave function will be symmetric (bosonic). At $finite$ temperatures, these competing exchange effects in the real-space wave function may cancel to a significant extent in the case of spin-$\frac{1}{2}$ fermions. Moreover, the critical molar volume is larger for ^{3}He than for ^{4}He, which also tends to reduce the importance of exchange in ^{3}He.

Besides the neglect of exchange effects, there are three additional sources of errors that need to be addressed: statistical errors, finite time-step discretization errors, and errors due to finite Trotter numbers. For all figures presented in Sec. III, these errors are smaller than or at most of the order of the symbol size. Typically, the statistical errors are smaller than 1% in both volume and energy. In the immediate vicinity of the phase transition, the statistical errors are about five times larger. The extrapolation $M \to \infty$ adds another 0.5% of uncertainty, again increased by a factor of 5 in the immediate vicinity of the phase transition. The time-step discretization error was found to be much smaller than the statistical error at both the lowest and the highest investigated temperatures. Indeed, these two limiting cases impose the most severe constraints on Δt: At low temperatures, in the isobaric ensemble, the density and hence the elastic modulus are relatively large, leading to large "Debye frequencies," thus requiring small time steps. At high temperatures, small time steps are required by the strong collisions, because the atoms deeply penetrate the repulsive parts of the potential, leading to sudden changes in the trajectories. Since Δt is sufficiently small in either case, we can safely assume it to be so over the entire temperature range. In summary, when it comes to comparison to experiment, we expect that, apart from finite-size effects near criticality, the neglect of exchange interactions introduces the largest errors.

B. Virial expansion

An alternative method for calculating thermodynamic properties of quantum gases is by means of the quantum virial expansion. In the original approach (see Ref. 13, Chap. 6 and references therein), a series expansion in $\hbar$ is obtained for every virial coefficient. Here, a more efficient technique is used,[30–32] which is briefly outlined below.

The first correction to the internal energy of an ideal gas

arises from the pair interaction $u_{12}(\beta,V)$ of (quantum-mechanical) particles. A pair of particles is described by a center of mass mode, which can be treated classically in the second-order virial expansion, and the relative coordinate $\mathbf{r}$, which is confined to a (spherical) volume V. Throughout the derivation, finite-volume corrections are ignored. For $N^2/2$ particle pairs, $U(N,V,\beta)$ becomes[17]

$$U(N,V,\beta)=\frac{3N}{2\beta}+\frac{N^2}{2}u_{12}(\beta,V)+\mathcal{O}\left\{N\left(\frac{N}{V}\right)^2\right\}, \qquad (4)$$

where $u_{12}(\beta,V)$ is calculated according to

$$u_{12}(\beta,V)=-\frac{\partial}{\partial\beta}\log\int_V d^3r\,\langle\mathbf{r}|e^{-\beta(\hat{t}_{\mathrm{rel}}+\hat{v}_{12})}|\mathbf{r}\rangle$$

$$+\frac{\partial}{\partial\beta}\log\int_V d^3r\,\langle\mathbf{r}|e^{-\beta\hat{t}_{\mathrm{rel}}}|\mathbf{r}\rangle, \qquad (5)$$

where $\hat{t}_{\mathrm{rel}}$ denotes the operator for the kinetic energy associated with the *relative* motion of two particles and v_{12} is their potential energy. The two integrands on the right-hand side of Eq. (5) are the diagonal elements of the density matrix $\rho(\mathbf{r},\mathbf{r}',\beta)$

$$\rho(\mathbf{r},\mathbf{r}',\beta)=\langle\mathbf{r}|\exp[-\beta(\hat{t}_{\mathrm{rel}}+\hat{v}_{12})]|\mathbf{r}'\rangle, \qquad (6)$$

and of its noninteracting counterpart.

Up to a normalization factor, which is irrelevant for the calculation of $u_{12}(\beta,V)$ in Eq. (5), the radial distribution function $g(r)$ is given by the diagonal elements of $\rho(\mathbf{r},\mathbf{r}',\beta)$. Taking into account that $\int_V d^3r\,g(r)\to V$ in the thermodynamic limit, it is possible to rewrite Eq. (5) in the more familiar form

$$u_{12}(\beta,V)=\frac{2}{V}\frac{\partial B_2(\beta)}{\partial\beta}, \qquad (7)$$

where, like for classical systems, the second virial coefficient $B_2(\beta)$ can be expressed in terms of $g(r)$

$$B_2(\beta)=-2\pi\int_0^\infty dr\,r^2\,[g_{12}(r)-g_0(r)]. \qquad (8)$$

Here, $g_{12}(r)$ and $g_0(r)$ denote the radial distribution function in the interacting and noninteracting case, respectively.

The diagonal elements $\rho(\mathbf{r},\mathbf{r},\beta)$ can be calculated by exploiting the semigroup property of the density operator

$$\rho(\mathbf{r},\mathbf{r}',2\beta)=\int d^3r''\rho(\mathbf{r},\mathbf{r}'',\beta)\rho(\mathbf{r}'',\mathbf{r}',\beta). \qquad (9)$$

Thus, we can obtain the low-temperature density matrix at temperature T by squaring the density matrix at temperature $2T$. For n iterations, the starting temperature has to be chosen as $2^n T$. For the highest temperature of the iteration process, it is possible to use the so-called primitive decomposition for $\rho(\mathbf{r},\mathbf{r}',\beta/M)$, which underlies the path-integral simulations in this paper as well as most other path-integral simulations. One of the advantages of the squaring procedure over path-integral simulations is that the required numerical effort scales only logarithmically with inverse temperature. Hence, it is easy to minimize discretization errors (for two-particle systems) using squaring tech-
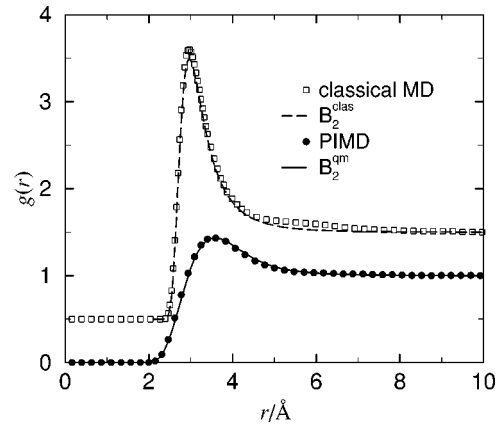

FIG. 1. Radial distribution function $g(r)$ for ^{4}He at temperature $T=10$ K and pressure $P=0.227\,46$ MPa, as obtained from both classical and quantum-mechanical calculations. The points result from simulations, while lines indicate second-order virial expansions. For clarity, the classical curves have been raised by 0.5.

niques at low temperatures. At a given (high) temperature, the systematic error is proportional to $1/M^2$, just as in path-integral simulations.[29]

For spherically symmetrical potentials, Eq. (9) can be reduced to a sum of one-dimensional integrations by decomposing the density matrix into contributions belonging to different angular momenta.[30,31] In practice, the squaring is done in terms of simple matrix multiplication by discretizing the variable r. Of course, a cutoff r_c has to be introduced at a reasonably large value of r. This induces artificial behavior at the boundary not found in an infinitely large system, namely that $g_0(r)$ tends to zero as r approaches r_c. Therefore, the integration in Eq. (8) has to be confined to the region where boundary effects are negligible. Alternatively, one may normalize the integrand in Eq. (8) by $g_0(r)$, which results in a fast convergence of B_2 with r_c.

Quantum effects in the calculation of $B_2(\beta)$ will become important when the thermal wavelength $\lambda(\beta)=h/\sqrt{2\pi m k_B T}$ of the free particle is of the order of or larger than the distance at which the interatomic potential is minimum. However, this is a rather qualitative criterion, and one might argue that quantum effects become important already when $\lambda(\beta)$ is of the order of the hard-sphere diameter, i.e., at four times higher temperatures. We illustrate this in the case of ^{4}He at a temperature $T=10$ K, where $\lambda\approx2.8$ Å. In Fig. 1, the two-particle radial distribution function $g(r)$ is shown for a pair of "classical" helium atoms and a pair of ^{4}He atoms. The maximum in $g(r)$ for the quantum-mechanical calculation is shifted by about 0.59 Å with respect to the classical equilibrium distance and the height of the maximum (relative to $g_0=1$) is decreased by a factor of about 5.8. Thus, an effective classical potential $V_{\mathrm{eff}}(r)$ that would result in a similar $g(r)$ of ^{4}He at $T=10$ K as the quantum-mechanical calculation would have a strongly reduced binding energy with respect to the original Aziz potential and an equilibrium distance shifted by 0.59 Å. Note that also the curvature of the effective potential would be different from the original potential.

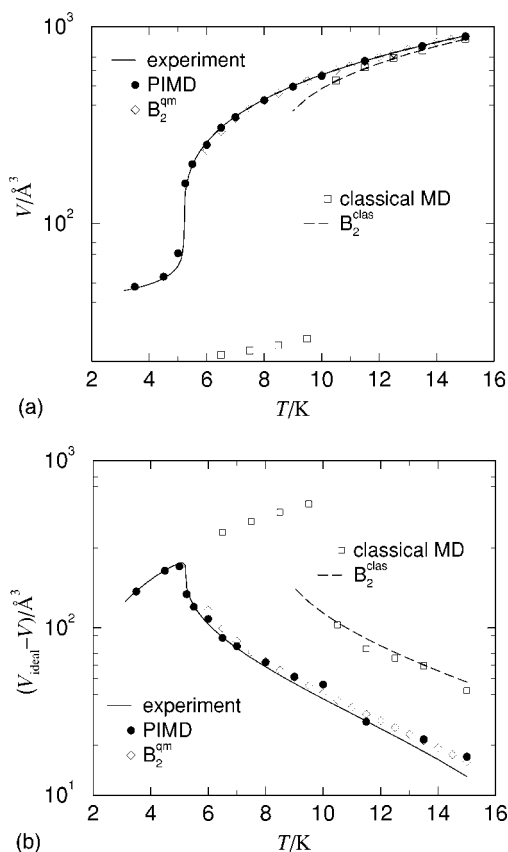In Fig. 1, PIMD simulation results, taken at the same

FIG. 3. Kinetic energy (positive values) and potential energy (negative values) for ^{4}He as a function of temperature T, at a pressure $P = 0.227\,46$ MPa. Points result from simulations, while the solid curves result from the second-order virial expansion. The dashed line indicates the classical kinetic energy.

FIG. 2. (a) Volume V per atom for ^{4}He (experiments correspond to the solid line, PIMD data to the circles, and the second-order quantum-mechanical virial expansion to the diamonds) and for "classical helium" (classical MD data correspond to the open squares and the classical virial expansion to the dashed line) as a function of temperature at the critical isobar of ^{4}He ($P_{c,4}$ $= 0.227\,46$ MPa). (b) The same symbols as in (a), but now the difference between the ideal gas volume $V_{\text{ideal}} = k_B T/P$ and the actual volume per atom is shown as a function of temperature.

temperature and the critical pressure $P_{c,4} = 0.227\,46$ MPa,[33] are included as well. The agreement between the virial expansion and the simulation is very good. For the classical system, small differences in $g(r)$ can be seen between both methods that can be attributed to three-body effects, which are neglected in the second-order virial expansion.

III. RESULTS

A. Critical isobar of ^{4}He

As a first test of the PIMD simulation and the virial expansion, we have calculated the atomic volume as a function of temperature on the critical isobar, $P_{c,4} = 0.227\,46$ MPa.[34] While for ^{3}He the diameter $\rho_d = (\rho_{\text{liq}} + \rho_{\text{vapor}})/2$ has a slope that is almost zero,[35] for ^{4}He it has a clearly positive slope. Thus, while the isobaric thermal expansion coefficient $V^{-1}(\partial V/\partial T)_P$ only has a finite peak as a function of temperature for $P > P_c$, it diverges at the liquid–vapor transition temperature for $P \leqslant P_c$. The results for classical and quantum-mechanical calculations are presented in Fig. 2 and comparison is made to a phenomenological wide-range equation of state based on experimental data.[34,36] As can be seen, the overall agreement between the experimental results and the quantum-mechanical simulations is very good. Indeed,
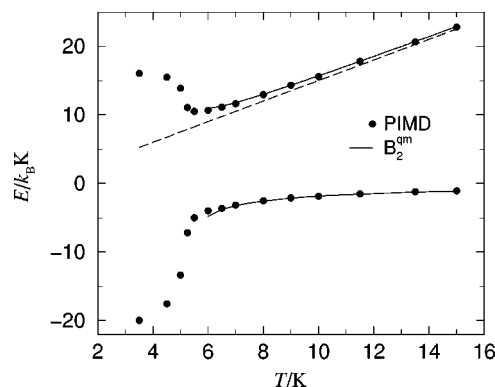
the discrepancies are considerably smaller than one might have inferred from the discussion in Sec. II A, and it cannot be excluded that to some extent there is a fortuitous cancellation of errors arising from the finite system size, the introduction of a cutoff radius, and imperfections in the potential. Only near the critical temperature, $T_{c,4} = 5.1953$ K,[34] small systematic deviations occur, which however may be tentatively attributed to finite-size effects in the simulations. In addition, the performance of the phenomenological equation of state itself might deteriorate in the critical region. The second-order quantum virial expansion, included in the same figure, exhibits deviations from the experimental curve below a temperature of approximately 7 K.

For comparison, data for "classical helium" are included in Fig. 2 as well. The absence of quantum fluctuations leads one to expect an increase in both the critical temperature and the critical pressure. Thus, the classical system should undergo a first-order phase transition at the critical pressure $P_{c,4}$, as is indeed borne out by the numerical data. The corresponding transition temperature T_1 could be located at approximately 10 K; here, both the fluid and the gas phase were stable for the duration of the simulation. Hysteresis effects and, possibly, slowing down owing to the vicinity of the critical point, may have affected the accuracy of this estimate. Since neither the pressure $P_{c,4}$ nor the corresponding transition temperature play a particular role for the classical system, no further attempts were made to improve the estimate of T_1. We note only that the *critical* temperature $T_c^{\text{class}} > T_{c,4}$ of the classical system will be even higher than T_1. The magnitude of the shift of the transition temperature is a clear indication of the importance of quantum-mechanical effects in the vicinity of the critical point. Indeed, from the principle of corresponding states[13] one finds (approximating the interaction potential by a Lennard-Jones potential with $\sigma = 2.56$ Å and $\varepsilon/k_B = 10.22$ K, Ref. 13) $T_c^{\text{class}} = 13$ K and $P_c^{\text{class}} = 1.1$ MPa.

An interesting effect can be observed in the kinetic energy T_{kin} for ^{4}He, shown in Fig. 3. Upon lowering the temperature, T_{kin} suddenly rises in the vicinity of the critical temperature. This rise is purely related to the increase in the
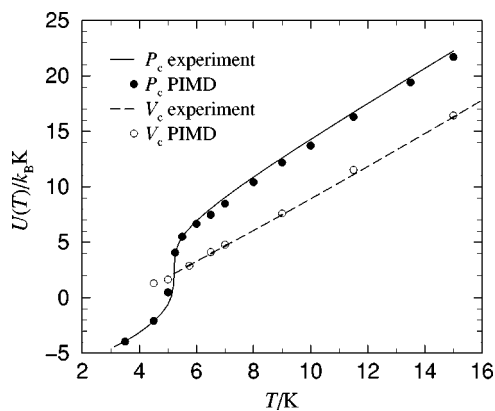
FIG. 4. A comparison of experimental and numerical results for the internal energy of ^{4}He as a function of temperature, both along the critical isobar (solid curve and closed circles, respectively) and along the critical isochore (dashed line and open circles, respectively). In both cases, the agreement is good.

FIG. 5. The kinetic (positive values) and potential (negative values) energy per atom for ^{4}He as a function of temperature T, along its critical isochore. Points result from simulations (closed circles for the quantum-mechanical calculations and open squares for the classical ones), while the solid curves result from second-order virial expansions. The dotted and the dashed curves indicate second- and third-order virial expansions, respectively, for the classical potential energy.

density of the system. It should be noted that the behavior of T_{kin} close to T_c is likely to be affected by finite-size effects, as these effects generally shift the top of the coexistence curve toward temperatures *above* the true critical temperature. The breakdown of the second-order virial expansion due to this increase in density occurs already slightly above $T_{c,4}$, namely around 5.5 K. The potential energy V_{pot}, depicted in the same figure, increases with temperature, as usual. We note, however, that this tendency of decreasing kinetic energy and increasing potential energy upon increase of the temperature near T_c is not a necessity: A quantum-mechanical model for molecular ordering of rotors on a surface rather showed the opposite trend, where $\langle T_{\text{kin}} \rangle$ increased and $\langle V_{\text{pot}} \rangle$ decreased near T_c upon increasing temperature.[37]

Figure 4 shows the *internal* energy along the critical isobar, both as obtained from experiment[34,36] and as calculated by means of PIMD. Although the experimental data lie systematically above the numerical ones for $T > 6$ K, the overall agreement is certainly appreciable.

Finally, we mention that the average *classical* potential energy $\langle V_{\text{pot}} \rangle$, which is not shown in Fig. 3, exhibits a clear jump, as expected for a first-order transition.

B. Critical isochore of ^{4}He

We now turn to the critical isochore, $\rho_{c,4} = 0.017\,399$ mol/cm^3.[34] Figure 5 shows both the kinetic and the potential energy per atom, along with the results of the quantum virial expansion. As can be seen, the agreement is remarkably good for the kinetic energy, even in the critical region. For the potential energy, on the other hand, the agreement is not so good, even at relatively high temperatures. In the same figure, we have also included the potential energy for "classical helium," as obtained from the second-order and third-order virial expansions: Here, the agreement is much better. However, a remark on the density is in order here. As mentioned before, quantum fluctuations generally lead to a lower critical temperature and hence, at the same pressure, to a higher density. However, the *critical* pressure decreases, and the net effect is that fluids in which quantum-mechanical effects are
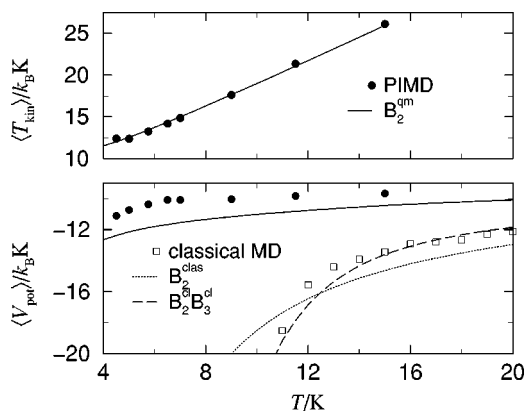
non-negligible have a *lower* critical density than would be expected from the principle of corresponding states.[13] This is also nicely illustrated by the critical properties of ^{3}He, which is basically described by the same pair potential as ^{4}He, but has an even lower critical temperature, pressure, and density, entirely due to its lower mass and consequentially larger de Boer parameter.[12] Indeed, a quantum-mechanical version of the principle of corresponding states can be formulated, in which all deviations from classical behavior are parametrized by this parameter.[13] From this slight digression, we conclude that the classical data, as shown in the figure, pertain to an isochore that is (for the *classical* system) a subcritical one, which might (in addition to the higher order of the virial expansion) explain the quite reasonable agreement. One remaining point, then, is that this isochore must cross the vapor branch of the coexistence curve at an unknown temperature.

Just like along the critical isobar, the PIMD results for the internal energy along the critical isochore (Fig. 4) exhibit good agreement with the experimental data.

C. Critical isochore of ^{3}He

Finally, we consider ^{3}He on its critical isochore, $\rho_{c,3} = 0.013\,74$ mol/cm^3.[35] Figure 6 shows both the kinetic and the potential energy per atom as obtained from PIMD simulations and from the second-order quantum virial expansion. As for ^{4}He, the agreement between both types of calculations is very good for the kinetic energy and rather poor for the potential energy. Also, the overall behavior of both energies is similar to that found for ^{4}He, except that in Fig. 6 one cannot observe the formation of a "plateau" in $\langle T_{\text{kin}} \rangle$ at lower temperatures. This is presumably due to the fact that the simulations for ^{3}He do not quite reach the critical temperature, $T_{c,3} = 3.317$ K (see Ref. 35; the value was converted to the T_{90} temperature scale here), where the flattening of the curve is expected to set in.

In principle, one might use the kinetic energy to define an effective, nonlinear temperature scale in which the role of the quantum fluctuations has been taken into account. By
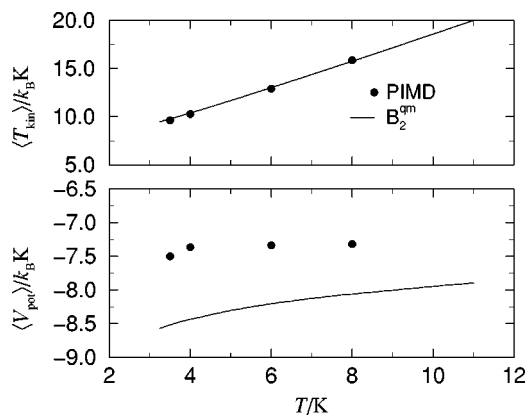
FIG. 6. The kinetic (positive values) and potential (negative values) energy per atom for ^{3}He as a function of temperature, along its critical isochore. The closed circles were obtained by means of simulations and the solid curves represent second-order virial expansions.

studying the crossover scaling function for, e.g., the compressibility on such a redefined temperature scale, one could examine the role of quantum effects in the deviations observed in Ref. 11. However, the definition of such a temperature scale requires a very accurate knowledge of the kinetic energy, in particular for temperatures very close to T_c, since crossover scaling functions are studied on a logarithmic scale in the reduced temperature t. Unfortunately, the numerical accuracy of our PIMD data did not warrant a meaningful, direct reexamination of the crossover scaling functions. As an alternative, we provide here qualitative evidence justifying the conjecture of Ref. 11 that the influence of quantum effects changes appreciably within the crossover regime. To this end, we have considered the effective potential V_{eff} as defined by

$$e^{-\beta V_{\text{eff}}(r)} \equiv g(r), \tag{10}$$

where $g(r)$ is the two-particle correlation function. The latter quantity, in turn, can be obtained from the virial expansion. Both V_{eff} and $g(r)$ are temperature-dependent quantities. The resulting effective potential is shown in Fig. 7 for three dif-
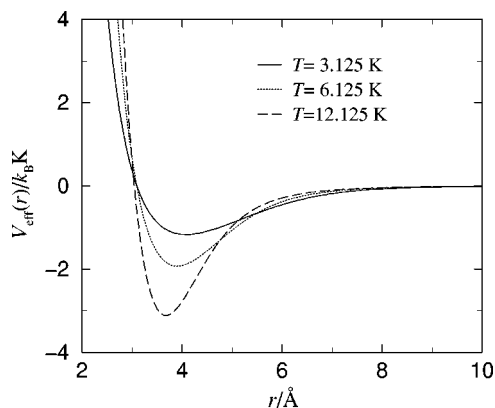

FIG. 7. Effective potential for ^{3}He as obtained from the quantum virial expansion, for three different temperatures. One observes the deepening and narrowing of the potential well when the temperature is increased from $T \simeq T_{c,3}$ to $T \simeq 4T_{c,3}$. The Aziz HFD-B potential (Ref. 27) takes its minimum at $r = 2.963$ Å.

ferent temperatures, namely $T = 3.125$ K (just below T_c), $T = 6.125$ K (roughly twice T_c), and $T = 12.125$ K (somewhat above the highest temperature studied in Ref. 11). One observes that the effective potential changes rather dramatically under this temperature variation: The depth of the potential well decreases by roughly a factor of 3 when the temperature is reduced from 12.125 to 3.125 K, and its width increases accordingly. This is in concordance with the observed enhancement of the compressibility over this temperature region. We note that, in a similar spirit, the effect of a temperature-dependent effective potential has been discussed earlier for a Lennard-Jones fluid;[31,32] however, no immediate connection with the second virial coefficient was made at that time.

IV. DISCUSSION AND CONCLUSION

In this paper, we have presented the results of a numerical study of ^{4}He and ^{3}He in the vicinity of their respective liquid–vapor critical points. Both path-integral molecular dynamics and quantum virial expansions have been applied.

For ^{4}He, we have shown that the Aziz potential[27] employed in the PIMD calculations yields very good agreement with experimental results[34,36] for the atomic volume at the critical isobar over a wide temperature range, including temperatures that lie considerably below the critical temperature. Equally good agreement is found for the internal energy. The second-order quantum virial expansion shows good agreement for the atomic volume down to roughly 2 K above the critical temperature. The simulations also demonstrate the importance of quantum effects in ^{4}He in the vicinity of its critical point: A classical system with the same potential has a critical temperature that is more than twice as high.

In addition, we have studied the kinetic and potential energy of ^{4}He and ^{3}He along their critical isochores. For the kinetic energy, there is good agreement between the quantum virial expansion and the simulation results in both cases, down to quite low temperatures, but for the potential energy the agreement is not so good. Higher-order terms in the virial expansion would probably alleviate the discrepancy, but are tedious to calculate. On the other hand, simulation results for the isochoric internal energy of ^{4}He agree well with experimental results.

One of our original goals was the definition of an effective, nonlinear temperature scale based on the kinetic energy. Such a temperature scale might prove useful for the reexamination of the crossover scaling functions of helium, which were experimentally observed to differ qualitatively from their counterparts for other simple liquids; these deviations have been conjectured to originate from quantum-mechanical effects.[11] Indeed, since (part of) these effects would now be incorporated in the new temperature scale, the crossover scaling functions should exhibit a better agreement with the (classical) prediction if the conjecture were correct. However, it is very difficult to reach the required numerical accuracy in the kinetic energy; in addition, very large particle numbers are needed in the immediate vicinity of the critical point, in order to circumvent finite-size effects. Thus, we have opted for a different strategy, namely the calculation of

the effective pair potential for ^{3}He by means of the quantum virial expansion evaluated on the critical isochore. We find that this pair potential exhibits a strong variation with temperature in the crossover region. This is in good accord with the conjecture of Ref. 11: Namely, not only are there strong quantum effects in ^{3}He close to its liquid–vapor critical point, as was already evident from the values of the critical amplitudes (cf., e.g., Ref. 35), but these quantum effects also *vary* considerably within the crossover region. Such a variation might then explain the observed apparent depression (relative to the predicted crossover scaling function) of the compressibility above T_c when the temperature is increased.

ACKNOWLEDGMENTS

[1] C. Bagnuls and C. Bervillier, Phys. Rev. B **32**, 7209 (1985).

[2] M. A. Anisimov, S. B. Kiselev, J. V. Sengers, and S. Tang, Physica A **188**, 487 (1992).

[3] E. Luijten, H. W. J. Blöte, and K. Binder, Phys. Rev. Lett. **79**, 561 (1997); Phys. Rev. E **56**, 6540 (1997).

[4] S. Caracciolo, M. S. Causo, A. Pelissetto, P. Rossi, and E. Vicari, Nucl. Phys. (Proc. Suppl.) **73**, 757 (1999).

[5] E. Luijten, Phys. Rev. E **59**, 4997 (1999).

[6] G. Meier, D. Schwahn, K. Mortensen, and S. Janßen, Europhys. Lett. **22**, 577 (1993).

[7] M. A. Anisimov, A. A. Povodyrev, V. D. Kulikov, and J. V. Sengers, Phys. Rev. Lett. **75**, 3146 (1995).

[8] Y. B. Melnichenko, M. A. Anisimov, A. A. Povodyrev, G. D. Wignall, J. V. Sengers, and W. A. Van Hook, Phys. Rev. Lett. **79**, 5266 (1997).

[9] M. A. Anisimov and J. V. Sengers, in *Equations of State for Fluids and Fluids Mixtures*, edited by J. V. Sengers, R. F. Kayser, C. J. Peters, and H. J. White, Jr. (Elsevier, Amsterdam, 2000).

[10] E. Luijten and K. Binder. Phys. Rev. E **58**, R4060 (1998); **59**, 7254(E) (1999).

[11] E. Luijten and H. Meyer, Phys. Rev. E **62**, 3257 (2000).

[12] J. de Boer, Physica (Amsterdam) **14**, 139 (1948).

[13] J. O. Hirschfelder, C. F. Curtiss, and R. Byron Bird, *Molecular Theory of Gases and Liquids* (Wiley, New York, 1954).

[14] E. Luijten and K. Binder, Europhys. Lett. **47**, 311 (1999).

[15] M. Rasolt, M. J. Stephen, M. E. Fisher, and P. B. Weichman, Phys. Rev. Lett. **53**, 798 (1984).

[16] P. B. Weichman, M. Rasolt, M. E. Fisher, and M. J. Stephen, Phys. Rev. B **33**, 4632 (1986).

[17] D. M. Ceperley, Rev. Mod. Phys. **67**, 279 (1995).

[18] D. M. Ceperley, R. O. Simmons, and R. C. Blasdell, Phys. Rev. Lett. **77**, 115 (1996).

[19] D. M. Ceperley and M. H. Kalos, in *Monte Carlo Methods in Statistical Physics*, Topics Curr. Phys. Vol. 7, edited by K. Binder (Springer, Berlin, 1979).

[20] K. E. Schmidt and D. M. Ceperley, in *The Monte Carlo Method in Condensed Matter Physics*, Topics Appl. Phys. Vol. 71, edited by K. Binder (Springer, Berlin, 1992).

[21] M. E. Tuckerman, B. J. Berne, G. J. Martyna, and M. L. Klein, J. Chem. Phys. **99**, 2796 (1993).

[22] R. P. Feynman and A. R. Hibbs, *Quantum Mechanics and Path Integrals* (McGraw-Hill, New York, 1965).

[23] D. Marx and M. H. Müser, J. Phys.: Condens. Matter **11**, R117 (1999).

[24] M. Herman, E. F. Bruskin, and B. J. Berne, J. Chem. Phys. **76**, 5150 (1982).

[25] P. Schöffel and M. H. Müser, Phys. Rev. B **63**, 224108 (2001).

[26] G. J. Martyna, A. Hughes, and M. E. Tuckerman, J. Chem. Phys. **110**, 3275 (1999).

[27] R. A. Aziz, F. R. W. Court, and C. C. K. Wong, Mol. Phys. **61**, 1487 (1987).

[28] S. Moroni, F. Pederiva, S. Fantoni, and M. Boninsegni, Phys. Rev. Lett. **84**, 2650 (2000).

[29] M. Suzuki, in *Quantum Monte Carlo Methods in Equilibrium and Nonequilibrium Systems*, edited by M. Suzuki (Springer, Berlin, 1987).

[30] R. G. Storer, J. Math. Phys. **9**, 964 (1968).

[31] D. Thirumalai, E. J. Bruskin, and B. J. Berne, J. Chem. Phys. **79**, 5063 (1983).

[32] E. L. Pollock and D. M. Ceperley, Phys. Rev. B **30**, 2555 (1984).

[33] The subscript "4" will generally be used to indicate quantities pertaining to ^{4}He, whereas a subscript "3" refers to ^{3}He.

[34] E. W. Lemmon, M. O. McLinden, and D. G. Friend, in *NIST Chemistry WebBook, NIST Standard Reference Database Number 69*, edited by W. G. Mallard and P. J. Linstrom (National Institute of Standards and Technology, Gaithersburg, MD, 2000). See http://webbook.nist.gov

[35] C. Pittman, T. Doiron, and H. Meyer, Phys. Rev. B **20**, 3678 (1979).

[36] R. D. McCarty and V. D. Arp, Adv. Cryog. Eng. **35**, 1465 (1990).

[37] B. Hetény, M. H. Müser, and B. J. Berne, Phys. Rev. Lett. **83**, 4606 (1999).